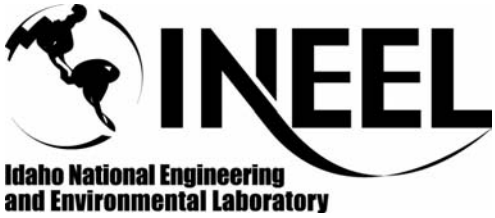

INEEL/CON-04-02258
PREPRINT

Boiling Visualization And Critical Heat Flux Phenomena In Narrow Rectangular Gap

J.J. Kim
Y.H. Kim
S. J. Kim
S. W. Noh
K. Y. Suh
J. L. Rempe
F. B. Cheung
S. B. Kim

November 28 – December 1, 2004

NTHAS4: Fourth Japan-Korea Symposium On Nuclear Thermal Hydraulics and Safety

NTHAS4: Fourth Japan-Korea Symposium on Nuclear Thermal Hydraulics and Safety
Sapporo, Japan, November 28 - December 1, 2004

BOILING VISUALIZATION AND CRITICAL HEAT FLUX PHENOMENA IN NARROW RECTANGULAR GAP

J.J. Kim[1], Y.H. Kim[1], S.J. Kim[1], S.W. Noh[1], K.Y. Suh[1*], J.L. Rempe[2], F. B. Cheung[3], S.B. Kim[4]

[1] Seoul National University
San 56-1 Sillim-dong, Gwanak-gu, Seoul, 151-742, Korea
*Phone: +82-2-880-8324, Fax: +82-2-889-2688, E-mail: kysuh@snu.ac.kr

[2]Idaho National Engineering & Environmental Laboratory
P.O. Box 1625, Idaho Falls, ID 83415, USA

[3]The Pennsylvania State University
304 Reber Building, University Park, PA 16802, USA

[4]Korea Atomic Energy Research Institute
P.O. Box 105, Yuseoung, Taejon, 305-600, Korea

ABSTRACT

An experimental study was performed to investigate the pool boiling critical heat flux (CHF) on one-dimensional inclined rectangular channels with narrow gaps by changing the orientation of a copper test heater assembly. In a pool of saturated water at atmospheric pressure, the test parameters include the gap sizes of 1, 2, 5, and 10 mm, and the surface orientation angles from the downward facing position (180^o) to the vertical position (90^o), respectively. Tests were conducted on the basis of visualization of boiling phenomena in the narrowly confined channel and the open periphery utilizing a high-speed digital camera. It was observed that the CHF generally decreases as the surface inclination angle increases, and as the gap size decreases. In the downward facing position (180^o), however, the vapor movement was enhanced by the gap structure, which produced the opposing result, say, the CHF increases as the gap size decreases. Phenomenological characteristics regarding the interfacial instability of vapor layer were addressed in terms of visualization approaching the CHF. It was found that there exists a transition angle, above which the CHF changes with a rapid slope.

1. INTRODUCTION

A number of aspects of pool boiling heat transfer and critical heat flux (CHF) characteristics have been studied such as the effect of surface orientation and gap size. The benefits of these studies have yielded a great deal of applications including cooling of the electronic and power appliances, heat treatment of metallic parts, and cooling of superconductor coils. In view of nuclear reactor safety management, it is crucial to accurately predict CHF and phenomenological boiling dynamics. In the Three-Mile Island Unit 2 (TMI-2) accident, for instance, the lower part of the reactor vessel was overheated but then rather rapidly cooled down (Suh and Henry, 1996a, 1996b; Kim and Suh, 2000). It was suggested that this rapid cooldown may have been due to cooling in a narrow gap, smaller than the order of centimeters that may have formed between the solidified core debris and the reactor vessel lower head. Experimental investigations are underway to quantify the CHF associated with bubble behavior that may affect the entire state of the heat transfer mode. Various two-phase flow patterns are also being observed to gain insights about the fundamental physics required to interpret the data. The CHF test sections are built to allow determination of the heat removal capability in both the confined and open channels.

2. BACKGROUND

Quite a few experimental studies have been done concerning the heater surface orientation, in which several researchers have tried to interpret the CHF mechanism for pool boiling by correlating the CHF data into a generalized equation (Chang and You, 1996; El-Genk and Guo, 1993; Howard and Mudawar, 1999) and for flow boiling circumstance (Galloway and Mudawar, 1993; Gersey and Mudawar, 1995). Among them, El-Genk and Guo (1996) developed the following CHF correlation for water that considers orientation

$$q_{CHF} = \left[0.034 + 0.0037(180-\theta)^{0.656}\right]\rho_g h_{fg} \cdot \left[\sigma(\rho_f-\rho_g)g/\rho_g^2\right]^{0.25} \quad (1)$$

Some researchers mentioned the existence of a transition angle at which the CHF decreases rapidly (Howard and Mudawar, 1999; Yang *et al*., 1997).

Also, many investigators have attempted to predict the gap size effect on the CHF in various channels. Several correlations were generated in terms of the predominant functional variables (Chang and Yao, 1983; Chyu, 1988; Katto and Kosho, 1979; Monde *et al*., 1982). With the aid of dimensional analysis developed by Katto (1978), the following correlating equation can be obtained for the CHF during natural convective boiling in confined channels in the near-vertical region

$$\frac{q_{CHF}/\rho_g h_{fg}}{\sqrt[4]{\sigma g\sin(\theta)(\rho_f-\rho_g)/\rho_g^2}} = \frac{C_1}{1+C_2\left(\rho_f/\rho_g\right)^{C_3}\left(g\sin(\theta)(\rho_f-\rho_g)s^2/\sigma\right)^{C_4}\left(D_h/s\right)} \quad (2)$$

where $D_h = \frac{2wl}{w+l}$ is the equivalent heated surface diameter.

Monde *et al*. (1982) carried out CHF experiments with a copper plate in the vertical rectangular channel with gap sizes ranging from 0.45 to 7.00 mm. They correlated their CHF data with corresponding l/s being less than 120 in four test liquids: water, ethanol, R-113 and benzene within 20% as

$$\frac{q_{CHF}/\rho_g h_{fg}}{\sqrt[4]{\sigma g(\rho_f-\rho_g)/\rho_g^2}} = \frac{0.16}{1+6.7\times10^{-4}\left(\rho_f/\rho_g\right)^{0.6}(l/s)} \quad (3)$$

The CHF triggering mechanism yet defies full understanding primarily due to the complexity of the effect of surface inclination and gap size. Hence, the current study was performed to predict the CHF in confined channels by rotating the test specimen. Results were obtained in the vicinity of the CHF as well as in the nucleate boiling regime utilizing the GAMMA 1D (Gap Apparatus Mitigating Melt Attack One Dimensional) apparatus at the Seoul National University.

3. EXPERIMENTS

3.1 Test Apparatus and Conditions

A heater assembly was fabricated utilizing the copper block test heater and the thin film resistor, which were designed first to facilitate use of the state-of-the-art devices for visualization of the vapor behavior, and second to avoid use of the direct current capacity exceeding 10A. A copper block belonging to the heater assembly had the wetted surface of 15×35 mm^2 in width by length, in which thin film resistor having resistance of 20W was affixed. A schematic diagram of the copper block heater is illustrated in Figure 1, where three chromel-alumel (K-type) thermocouples for measuring the temperature data on the wetted surface were inserted into the hole off the wetted surface by 0.6 mm and the depths of 5, 17.5 and 30 mm in the direction of the flow channel, respectively. Essentially, the test heater was slightly coated with nickel to prevent the test heater from being oxidized.

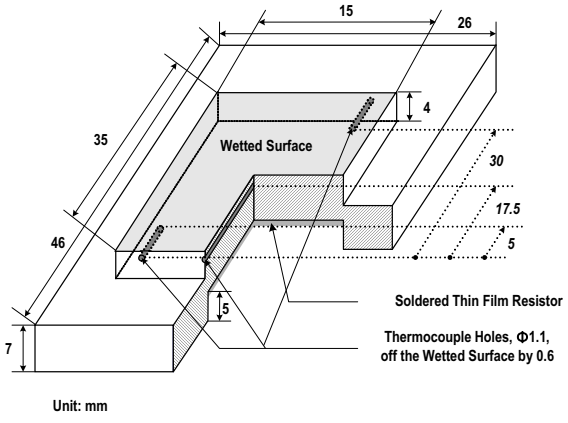

Fig. 1 Schematic diagram of test heater block

Regarding the device holding the heater assembly, the stainless steel housing was designed to ensure the most effective insulation on the heated section, as illustrated in Figure 2. In order to efficiently insulate the heated section, the interior of the housing is evacuated, and the inner surface of the housing is polished smoothly. The insulation efficiency is surprisingly high for vacuums of 10^{-4} torr, and such vacuums sizably reduce the heat loss from the bottom of the copper block heater. Pyrex glass was imbedded into the edge of the housing and designed to precisely maintain the gap sizes of 1, 2, 5 and 10 mm, and to visualize the test apparatus having a narrow rectangular channel, as demonstrated in Figure 2. Without the Pyrex guide shown in Figure 2, the same structure of the heater assembly was introduced for pool boiling in an open periphery experiment.

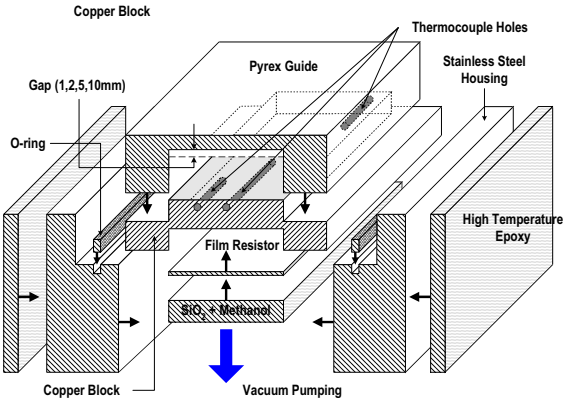

Fig. 2 Cross-sectional view of test heater assembly (Gap sizes: 1, 2, 5, and 10 mm)

In the same way as the housing, the water pool shown in Figure 3 was maintained at atmospheric pressure for the purpose of insulation. Two stainless steel tanks replenish the water pool, and the space between these tanks is maintained at low pressure by vacuum pumping. Hence, this functioned to sustain a steady thermodynamic state of water at atmospheric pressure, in which eight immersion type heaters having the electric capacity of 2 kW were homogeneously inserted into the test pool to pre-heat the demineralized water in the test pool up to saturation. A reflux condenser was equipped in the test pool itself to maintain the pressure in the water pool.

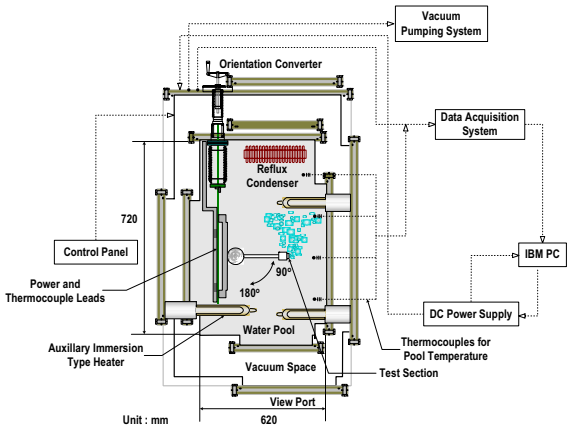

Fig. 3 Front view of vacuum water pool

3.2 Test Procedure and Data Reduction

The experimental procedure is explained below (see Figure 3). First, the heater surface was cleaned with acetone prior to each test. The pool was deaerated by running immersion-type heaters at the atmospheric saturated boiling condition for at least an hour prior to reading the data. Although this study is focused on the quantitative investigation of CHF, data in the nucleate boiling regime prior to CHF were also obtained.

Maintaining the thermodynamically saturated condition at atmospheric pressure, the heat flux was gradually increased utilizing a direct power supply.

At each stage, vapor behavior in the confined channels and open periphery was photographed through the view port using a high speed digital camera at 4000 fps, in which a high capacity light source provided illumination for high speed photography. Together with visualization, the heated surface temperature was

monitored using HP VEE5.0 and stored in data file format. While monitoring the temperature, CHF was judged to occur when the surface temperature rose in a rapid slope. The CHF was determined as the highest average heat flux that gave a stable temperature reading plus one half of the last average power increment (~3% of the CHF). In order to protect the thin film resistor from burnout, the electrical power was turned off immediately after the surface temperature reached 190°C.

After appropriate analysis of the heat flux and temperature data, the CHF values were determined for all the orientation angles within ±5%. In calculating the uncertainties associated with the experimental data, propagation of error was utilized. The K-type thermocouples were calibrated for a maximum uncertainty of ±0.1 degree C. The uncertainty in the heat flux due to instrumentation limitations was estimated to be within 1%. As mentioned earlier, this study adopted the vacuum pumping method to prevent the generated heat from getting lost from the sides other than that adjacent to the working fluid. Hence, the heat loss was considered to be negligible enough to ascertain full energy transfer from the heated surface to the working fluid.

4. RESULS AND DISCUSSION

4.1 Pool and Gap Boiling Visualization in Inclined Region

Fundamental characteristics of pool boiling environment can be extended to understanding of gap boiling. Hence, in order to understand the relationship between the two kinds of boiling states, this study used a one-dimensional test heater assembly with and without the gap structure.

Figures 4 and 5 show the typical pool boiling phenomena at inclined upward and downward locations, i.e. 45° and 135°, respectively. In addition, Figure 6 presents the narrow gap boiling bubble behavior in terms of the heat flux reaching the CHF at the same circumstances for the confined channel of 5 mm gap.

Comparing Figures 4 and 5, the former suggests that the free escape of vapor from the wetted surface of the test heater is driven by buoyancy rather than convection, whereas the latter suggests that the movement of bubbles is restricted by geometrical location due to gravity (e.g, bubbles are momentarily taken off the surface by the momentum of vapor generation and then escape from the region of the heated surface by buoyancy). For this reason, the approximate bubble diameter and overall size in the upward location are slightly larger than those in the downward location. On the other hand, most of the bubble growth and departure in Figure 6 is related to the competing gravitational and buoyant forces. This apparently explains the physical role of the gap structure, which can give an essential clue for insightful analysis of the pool and gap boiling phenomena. Compared to phenomena observed for pool boiling, confined channel bubble growth and coalescence are primarily due to the gap size effect associated with the gravitational and buoyant forces. In the vicinity of CHF, a stable vapor film is maintained, which results in sudden temperature escalation at the heated surface and finally, CHF.

In particular, the vapor layer thickness normal to the heated surface in the open periphery is greater than that in the 5 mm gap. This larger vapor film and free escaping vapor from the heater surface may explain the increased resistance against thermal attack at the heat removal surface. Accordingly, the CHF in the open periphery is larger than that in the 5 mm gap at a given surface inclination angle. Considering interrelation between CHF and heat transfer coefficient, however, this is not always directly related to larger heat transfer coefficients in the open periphery. The heat transfer coefficient in the vicinity of CHF in the open periphery at 95° inclination, for instance, is less than that in the 5 mm gap. Conversely, the CHF at such location is larger than that in the 5 mm gap. This may be attributed to the fact that the gap structure can give rise to higher mass flux compared with that in the open periphery. The gap structure can restrict the vapor growth toward the normal direction to the surface from which heat is removed. This in turn redirects the vapor velocity to become more parallel to the surface. Accordingly, the mass flux by restricting the gap structure can increase, and thus the higher mass flux can induce the higher heat transfer coefficient.

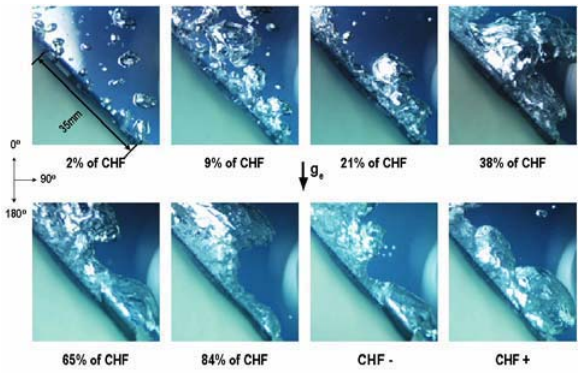

Fig. 4 Flow visualization (open periphery, 45°)

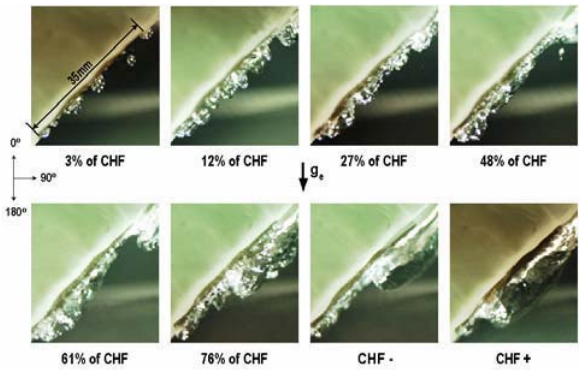

Fig. 5 Flow visualization (open periphery, 135°)

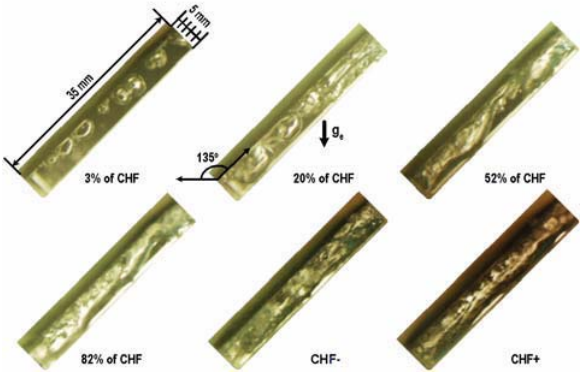

Fig. 6 Flow visualization (5 mm, 135°)

4.2 Pool and Gap Boiling Visualization in Vertical Region

Figure 7 demonstrates fundamental pool boiling characteristics photographed by the side and front of the test heater in the vertical location (90°). Figures 8, 9 and 10 present the bubble growth and coalescence in the 2, 5 and 10 mm gaps at the same location, respectively.

In analyzing two kinds of boiling states, the vapor behavior confined by the gap structure is more vigorous than in the open periphery, in which complexity of the flow mode may be due to the convective force resulting from the gap structure. However, inherently larger CHF in pool boiling than gap boiling will hold because the bubbles can escape from the channel more easily.

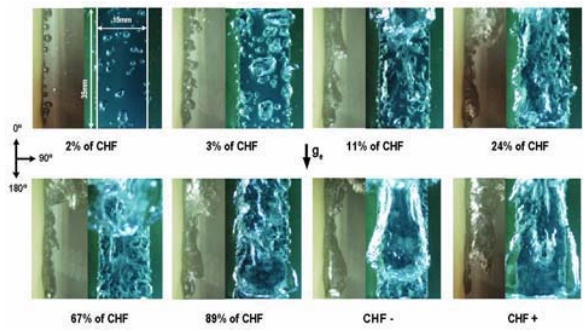

Fig. 7 Flow visualization (open periphery, 90°)

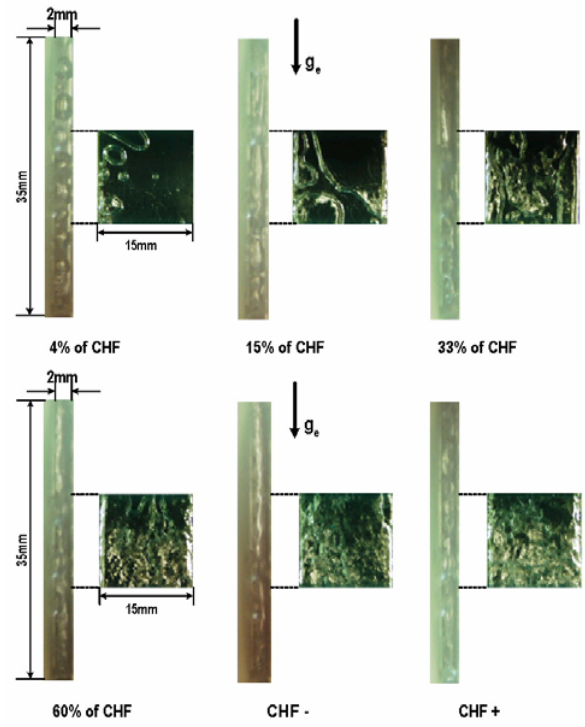

Fig. 8 Flow visualization (2 mm, 90°)

Note in Fig. 7 that the vapor motion right before the CHF, say, CHF-, exhibits typical pattern of the Helmholtz wavy motion. The convex vapor shape at bottom of vapor streak represents the higher vapor pressure. Conversely, the concave shape at top of vapor streak indicates the lower vapor pressure than liquid pressure, which may explain the inertial limited bubble growth in the vicinity of liquid. This limitation is determined by how rapidly it can push back the surrounding liquid. This also may give essential clue to determination of the critical wavelength. This is important in predicting the heat transfer rate. The reason is that the critical Helmholtz velocity can be calculated once the critical wavelength is experimentally and theoretically determined. Accordingly, this information can be utilized to determine the mass flow rate of the vapor phase.

Figures 8, 9 and 10 depict the typical gap boiling phenomena in the vertical channel, in which inherently larger bubble size compared with that of the refrigerant and cryogenic fluid plays an important role in triggering the CHF. In Figure 8, the vapor generation states are photographed as the heat flux increases. From the initial stage of boiling, bubbles are dispersed and coalesced due to narrow gap. As the heat flux increases, more vigorous vapor motions are observed and the liquid deficient fronts diminish. In the vicinity of the CHF, the vapor layer coalesced and dispersed by the individual vapor covers most regions of the channel, which induces relatively low CHF in the 2 mm gap compared with that in the open periphery. In case of visualization in the 10 mm gap, the average vapor layer thickness is larger than the gap size of 5 mm, say, about 6 mm and hence the seeming Helmholtz wavy motion in the 10 mm gap is disturbed by the gap structure in the 2 and 5 mm gap boiling. For the quantity of the CHF for each channel, the CHF increases as the gap size increases mainly due to the dominant buoyant force.

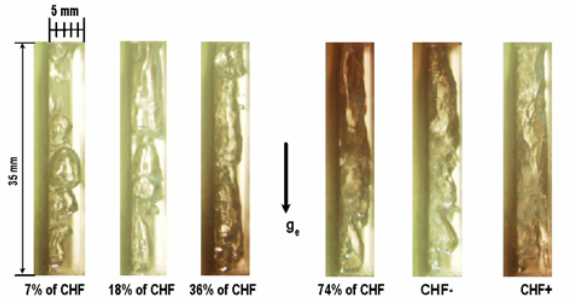

Fig. 9 Flow visualization (5 mm, 90°)

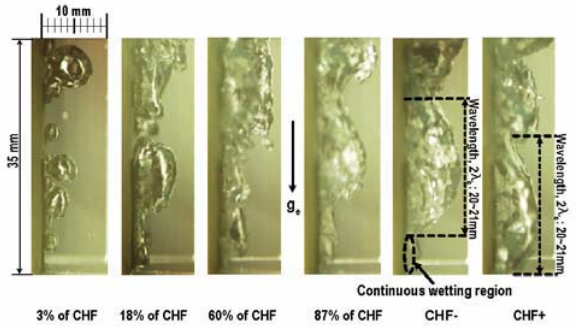

Fig. 10 Flow visualization (10 mm, 90°)

4.3 Gap Boiling Visualization in Downward-facing Region

Figures 11 and 12 present the two-phase flow visualization in the completely downward-facing location (180°), in which the gap sizes are 5 and 10 mm, respectively. In Figure 11, the bubbles in the gap are squeezed and dispersed in the vicinity of the CHF by the gap structure, and hence those tend to be ejected due to the induced flow effect. In Figure 12, on the other hand, the vapor layer thickness in the 10 mm gap is about 6~7 mm that is smaller than gap size of 10 mm. For the characteristic of completely downward-facing location (180°), the buoyant force is hampered significantly. Instead, the behavior is primarily affected by the momentum of the vapor rising from the wetted front. Thus, the vapor appears to be stagnated without escaping and this causes the lower CHF than in the 5 mm gap. This result repeats itself in the 1 and 2 mm gaps.

Table 1 presents the CHF associating with surface orientation angle and gap size. In vertical region (90°), the CHF increased as the gap size increased consistent with findings from several previous studies. In downward-facing region (180°), however, the opposing results were observed, i.e. the CHF increased as the gap size decreased.

4.4 Gap Size and Surface Orientation Effect

In Figure 13, several two-phase flow photographs in the vicinity of CHF are presented in terms of surface orientation angle in the 5 and 10 mm gaps. The snapshots help explain the combined effect of gap size and gravity in the rectangular channel.

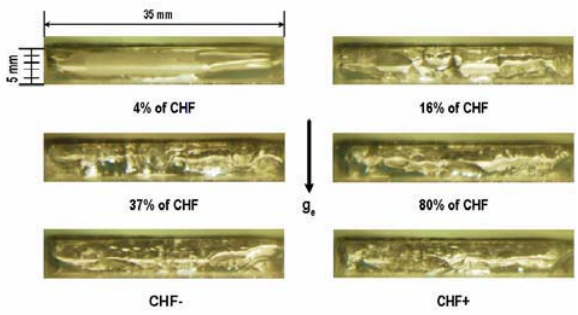

Fig. 11 Flow visualization (5 mm, 180°)

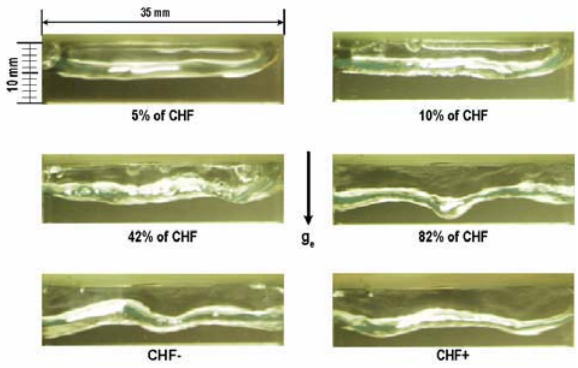

Fig. 12 Flow visualization (10 mm, 180°)

Table 1 CHF for Gap Size and Surface Orientation Angle (kW/m²)

Angle / Gap	90°	95°	105°	115°	125°	135°
1 mm	598.4	585.2	570.6	556.1	542.0	480.9
2 mm	984.6	969.4	954.3	937.2	900.5	860.3
5 mm	1,197	1,178	1,164	1,151	1,105	1,088
10 mm	1,204	1,189	1,153	1,120	1,062	1,025
Pool	1,341	1,320	1,310	1,244	1,276	1,189
Angle / Gap	145°	155°	165°	170°	175°	180°
1 mm	435.6	374.8	359.5	351.4	317.9	296.7
2 mm	803.3	702.6	526.5	448.2	369.8	282.0
5 mm	1049	972.3	876.9	793.5	646.7	228.7
10 mm	976.7	918.4	848.7	793.1	751.1	167.1
Pool	1,110	1,128	1,128	1,108	1,068	962.4

Visual inspection of fluid motion in the rectangular channel captured in Figure 13 revealed that the Helmholtz instability was not observed in the 1 and 2 mm gaps. In most surface inclinations of the 5 mm gap boiling, similar dispersed and coalesced vapor motion by the gap structure was detected excluding at certain inclination angles that may be interpreted as the Helmholtz instability motion. In the 10 mm gap boiling, however, the Helmholtz instability exists over the broad surface inclination angle. In particular, a wavelength of about 21 mm was observed at the vertical position (90°) in the 10 mm gap. Departing the angle of 180°, most of the vapor motions in the 10 mm gap have the characteristic of the Helmholtz instability near CHF, and this is typified in the vertical location. In the 5 mm gap boiling, however, the vapor movements are mostly induced by the gap in the completely downward-facing location (180°). This induced flow effect is weakened as the surface inclination approaches the vertical location (90°), in which buoyancy mainly affects the two-phase flow and accordingly the CHF.

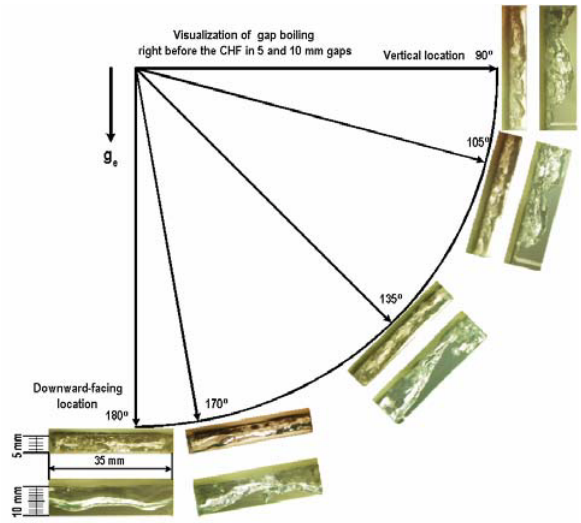

Fig. 13 Flow visualization at CHF- concerning surface orientation (5 and 10 mm)

Figure 14 presents the CHF data varying with the gap size and surface inclination angle. Figure 15 shows the CHF data for pool boiling with open periphery.

Until now it has generally been claimed that the CHF decreases as the gap size decreases. Contrary to this general belief, however, the present study has found opposing results at certain surface inclination angles. At the vertical location (90°), in consistency with the general belief, the CHF decreases as the gap size decreases. Especially, the CHF for the gap size of 10 mm is smaller than that for any other gap sizes at the fully downward-facing location (180°) as shown in Figures 14 and 15 and Table 1.

More detailed explanations shall shed light on understanding of the current finding that the CHF generally increases as the gap size increases, but the increasing rate decreases with an exception at the fully downward-facing angle as shown in Figure 14. The experimental data in this study are compared with other results reported in the literature. In the vertical rectangular geometry of Monde *et al*. (1982) and Xia *et al*. (1996), the increasing trend of the CHF with the gap size is compared with the present experimental data. It is found that the CHF changing trend differs with geometry. Though the overall behavior of CHF in the horizontal co-axial disk is comparable, the CHF is grossly overpredicted. Monde *et al*.'s correlation appears to reasonably represent the current experimental data. Accounting for the gravity effect in Equation (3), Monde *et al*.'s correlation is compared with the CHF in the gap and pool boiling as shown in Figure 15(a). While underestimating CHF for the 1, 2 and 5 mm gaps, their correlation satisfactorily predicts CHF for the 10 mm gap and pool boiling for most of the angles below, say, 150°.

Figures 15(a) and 15(b) demonstrate that the CHF for the 1 and 2 mm gaps decreases as the inclination angle increases and as the gap size decreases except at the fully downward-facing location (180°). As mentioned earlier, at the downward-facing angle, the bubble formed in the gap smaller than its thickness is affected by the induced flow due to the gap. To paraphrase, bubbles in the narrow gap can more easily escape from the restricted channel than those in the gap whose size exceeds the bubble thickness. Though the bubble in the 1, 2 and 5 mm gaps tends to be ejected due to the induced flow effect, the bubble in the 10 mm gap is stagnated. That is, the induced flow effect increases as the gap size decreases at the fully downward-

facing angle. Hence, at that location, the CHF decreases as the gap size increases contrary to the trend at other angles. However, the CHF in the pool boiling with the open periphery is greater than that in the gap boiling because the bubble in the pool boiling with open periphery is free to escape in the azimuthal direction.

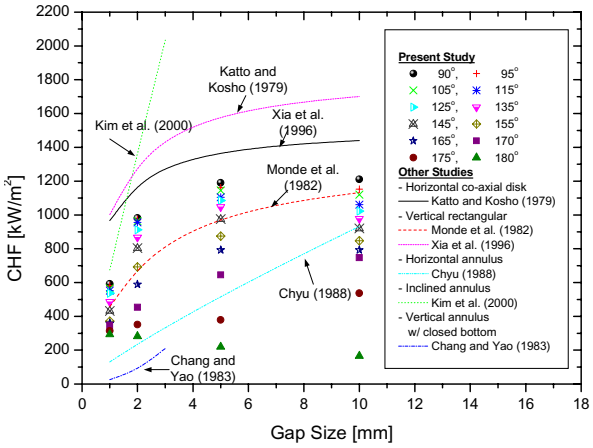

Fig. 14 Effect of gap size on the CHF

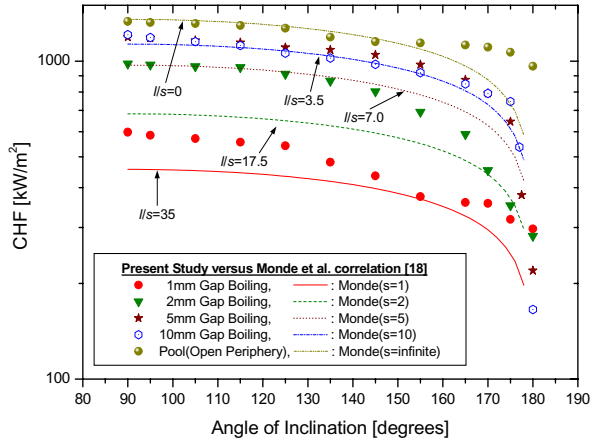

(a) Comparison against the Monde *et al.* Correlation

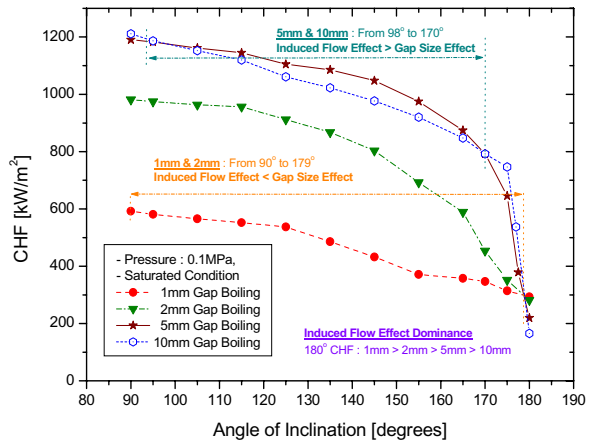

(b) Effect of induced flow and gap size on the CHF

Fig. 15 Effect of surface inclination angle on the CHF

While the CHF values for the 5 and 10 mm gaps both decrease as the inclination angle increases, the CHF for the 10 mm gap is less than that for the 5 mm gap over a wide range of angles due to absence of the induced flow effect in the 10 mm gap as portrayed in Figure 15(b). The flow rate depends on the balance between the driving force and the pressure drop. The driving force for the 5 mm gap is larger than that for the 10 mm gap due to high void fraction within the confined channel space. Given the flow rate, the pressure drop for the 5 mm gap is greater than that for the 10 mm gap. Then, the mass flux for the 5 mm gap can exceed that for the 10 mm gap due to the smaller flow area over a span of the inclination angles. Consequently, there can be a range of inclination angles over which the CHF increases as the gap size decreases. Interestingly enough, this newly theorized thermal hydraulic phenomenon appears to unmistakably take place at the fully downward-facing angle for all the gap sizes examined in this work, and occasionally over some range of angles for the 5 and 10 mm gaps. Therefore, the CHF in the gap boiling is affected by the gap size as well as by the induced flow within the gap.

4.5 Interfacial Instability Analysis

Mudawar *et al.* (1997) predicted and solved for the interfacial instability of vapor layer in vertical pool boiling by photographing the vapor layer for water as well as for FC-72 under the atmospheric pressure. They suggested the separated flow model and solved it analytically for some limiting cases, in which the average vapor velocity and critical wavelength were obtained. In the present study, a similar instability behavior at 10 mm gap boiling circumstance was detected as shown in Figure 10. More or less short heater length compared with several cycles of wavelength calculated from the classical instability theory, however, renders it hard to precisely determine its repeatability directly from the photograph. Although the repeated cycle of the instability behavior was not exactly discernable, wetting front propagation along a vertical surface can be predicted based upon the present photographic study and previous study of Mudawar *et al.* Figure 16 is a schematic diagram of the interfacial instability, where the leading edge at the bottom of the test heater is repeatedly wetted by the vapor generation.

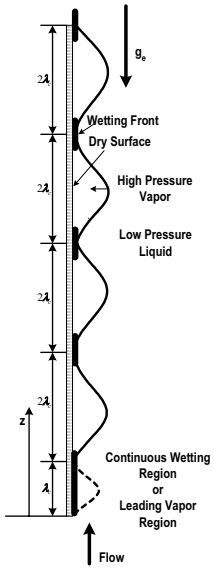

Fig. 16 Schematic diagram of interfacial instability

Away from the continuous wetting region in the leading edge, the wetting fronts are formed when a disturbance in the liquid-vapor interface becomes unstable during the growth of its amplitude until the interface contacts with the heater surface. Until reaching the CHF, wetting fronts keep in contact with the heater surface. In the vicinity of the CHF, however, the

momentum of the vapor generation overcomes the pressure force exerted on the liquid-vapor interface and thus the CHF takes place.

The pressure force plays an important role in perturbing the interfacial stability, while the momentum of the vapor generation tends to lift the wetting fronts off. The instability primarily occurs when the velocities differ between liquid and vapor. In the vertical pool boiling, the liquid and vapor velocities differ, whence the gravitational force may be weakened. With the aid of simple classical instability theory and the study of Mudawar *et al*., the critical wavelength in the 10 mm vertical gap boiling that is similar to the vertical pool boiling as well as the flow boiling, λ_c, was calculated based on the present experimental CHF data.

The classical hydrodynamic instability theory yields the critical length that renders the interfacial wave neutrally stabilized is given by

$$\lambda_c = \frac{2\pi}{k_c} = \frac{2\pi\sigma\left(\rho_f - \rho_g\right)}{\rho_f \rho_g u_g^{\ 2}} \tag{4}$$

In addition, integrating with respect to z after combining mass and energy conservations for the streamwise vapor layer length dz, gives

$$\rho_g u_g \delta = \frac{q_{CHF} z}{h_{fg}\left[1 + \frac{c_{p,f}\Delta T_{sub}}{h_{fg}}\right]} \tag{5}$$

On the same control volume, the momentum balance yields

$$\frac{d}{dz}\left[\rho_g u_g^2 \delta\right] = \left(\rho_f - \rho_g\right) g\delta - \tau_i - \tau_w\left(1 + \frac{2\delta}{w}\right) \tag{6}$$

Where the interfacial and wall shear stress, τ_i and τ_w, respectively, are defined as

$$\tau_i = 0.5 f_i \rho_g u_g^2 \tag{7}$$

$$\tau_w = 0.5 f_w \rho_g u_g^2 \tag{8}$$

In Equation (7), the interfacial friction factor, f_i, was presumably established constant value of f_i =0.5 that was offered by Galloway and Mudawar (1993), and Gersey and Mudawar (1995). They suggested that such value provided the best agreement between measured and predicted pressure drops obtained from flow boiling studies. Further, their parametric study of interfacial friction factor for vertical pool boiling gives an appreciation of the interfacial friction factor ranging from 0.25 to 1.0, which does not affect significantly the separated flow model. In Equation (8), the wall friction factor, f_w=0.0791/Re0.25, was set from the Blausius correlation for turbulent flow, in which the Reynolds number is based on the hydraulic diameter of the vapor layer, say, $2w\delta/(w+\delta)$.

Combining Equation (5) with Equation (6), one obtains a differential equation for vapor velocity u_g and axial location z. For some limiting cases such as where the wall shear stress and momentum gradient in Equation (6) are neglected, u_g would be approximated by

$$u_g = \left[\left(\frac{\rho_f - \rho_g}{\rho_g}\right)\frac{q_{CHF}}{0.5 f_i \rho_g h_{fg}\left[1 + \frac{c_{p,f}\Delta T_{sub}}{h_{fg}}\right]} gz\right]^{1/3} \tag{9}$$

In Figure 16, the first wetting front is referenced at $z=\lambda_c$. Hence substituting Equation (4) into Equation (9) with respect to the vapor velocity u_g for the $z=\lambda_c$ yields

$$\lambda_c = \left[2\pi\sigma\frac{\rho_f + \rho_g}{\rho_f \rho_g}\right]^{3/5} \cdot \left[\frac{\rho_f - \rho_g}{\rho_f \rho_g} g \frac{q_{CHF}}{0.5 f_i \rho_g h_{fg}\left[1 + \frac{c_{p,f}\Delta T_{sub}}{h_{fg}}\right]}\right]^{-2/5} \tag{10}$$

In the present study, experiment was conducted for the saturated water under the atmospheric pressure. Thus the liquid subcooling in Equation (10), ΔT_{sub}, should be set equal to zero. Moreover, the maximum heat flux can be replaced with the present experimental CHF data in the 10 mm gap boiling in the vertical region. Then, the final form of the critical wavelength equation is given by

$$\lambda_c = \left[2\pi\sigma\frac{\rho_f + \rho_g}{\rho_f \rho_g}\right]^{3/5} \cdot \left[\frac{\rho_f - \rho_g}{\rho_f \rho_g} g \frac{q_{CHF}}{0.5 f_i \rho_g h_{fg}}\right]^{-2/5} \tag{11}$$

The CHF in the 10 mm gap boiling at the vertical location is 1.204×10^6 W/m^2. The corresponding critical wavelength given by Equation (11) is 9.5 mm. Hence, $2\lambda_c$=19 mm, which is close to that shown in Figure 10.

5. CONCLUSION

In the present study, the CHF experiments were carried out for narrow gaps of 1, 2, 5 and 10 mm, in which the surface orientation effect was taken into account by varying the rectangular heater assembly having a heater length of 35 mm from vertical location (90^o) to downward-facing location (180^o) for distilled water under the atmospheric pressure. In addition, the experiment for pool boiling with open periphery was performed. While the quantitative CHF data were obtained by monitoring the temperature profile during experiments, at each stage of heat flux increase the two-phase flow movements were also photographed by using the high-speed digital camera. Several essential conclusions from the present study may be summarized as follows.

The visualization study both for the gap and pool boiling phenomena was conducted by using the high-speed camera devices. The pool and gap boiling in the inclined downward and upward-facing regions, 45^{o}and 135^o, was addressed in terms of the gravitational and buoyant forces. The pool and gap boiling in the vertical region, 90^o, was photographed approaching the CHF, in which the buoyant force dominates over all the other forces. The gap boiling characteristics were presented, in which the infeasibility of vapor escape gives rise to the lower CHF as the gap sizes increases.

The gap size and surface orientation effects play a crucial role in interpreting the general two-phase flow behavior as well as the CHF data. There exists a critical gap size commensurate to the average vapor layer thickness enhancing the heat transfer rate with increasing mass flux at certain surface orientation. Associated with the photographing study, the quantitative CHF data were obtained. It was observed that the CHF generally increases as the gap size increases, but the increasing rate decreases as the gap increases. In particular, the CHF in the gap size of 10 mm is smaller than the value at any other gap sizes at the fully downward-facing location (180^o). At the vertical location (90^o), as is generally believed, the CHF increases as the gap size increases. The CHF in gap boiling is affected by the gap size as well as by the induced flow within the channel.

There is a transition angle for each gap size. The transition angle increases as the gap size increases. The transition angles for the 2, 5 and 10 mm gap sizes were distinctly found to be 165^o, 170^o and 175^o, respectively.

ACKNOWLEDGEMENTS

This work was performed under the auspices of the Korean Ministry of Science and Technology (contract number M20112 000001-01B0300-00210) and the U.S. Department of Energy

(contract number DE-ACO7-991D13727) as an International Nuclear Energy Research Initiative project awarded to the Seoul National University and the Idaho National Engineering and Environmental Laboratory in collaboration with the Korea Atomic Energy Research Institute and the Pennsylvania State University.

NOMENCLATURE

C_1	constant in Equation (2)	
C_2	coefficient in Equation (2)	
C_3	exponent in Equation (2)	
C_4	exponent in Equation (2)	
$c_{p,f}$	specific heat of water	$[J/kg \cdot K]$
d	disk diameter	$[m]$
D_h	equivalent heated surface diameter	$[m]$
f	friction factor	
g	gravitational acceleration	$[m/sec^2]$
h_{fg}	latent heat of vaporization	$[J/kg]$
k_c	critical wave number	
l	heater length	$[m]$
q_{CHF}	critical heat flux	$[W/m^2]$
$q_{CHF,\,90^o}$	CHF in ordinary pool boiling at 90^o	$[W/m^2]$
s	channel gap size	$[m]$
u	average velocity	$[m/sec]$
w	channel width size	$[m]$
z	vapor layer length	$[m]$

Greek Letters

ΔT_{sub}	liquid subcooling	$[K]$
δ	vapor layer thickness	$[m]$
δ_v	vapor film thickness	$[m]$
θ	surface orientation angle (90^o: vertical, 180^o: downward-facing)	$[^o]$
ρ	density	$[kg/m^3]$
σ	surface tension	$[N/m]$
τ	shear stress	$[N/m^2]$
λ_c	critical wavelength	$[m]$

Subscripts

f	saturated liquid
g	saturated vapor
i	interfacial
w	wall

REFERENCES

Chang, J. Y. and You, S. M. (1996). "Heater Orientation Effects on Pool Boiling of Micro-Porous-Enhanced Surfaces in Saturated FC-72," *Transaction of ASME, Journal of Heat Transfer*, **118**, pp. 937-943.

Chang, Y. and Yao, S. (1983). "Critical heat flux of narrow vertical annuli with closed bottoms," *Journal of Heat Transfer*, **105**, pp.192-195.

Chyu, M. C. (1988). "Prediction of Boiling Dryout Flux for Restricted Annular Crevice," *International Journal of Heat and Mass Transfer*, **31**, pp. 1993-1998.

El-Genk, M. S. and Guo, Z. (1993). "Transient Boiling from Inclined Downward-Facing Surfaces in a Saturated Pool," *International Journal of Refrigeration*, **6**, pp. 424-432.

Galloway, J. E. and Mudawar, I. (1993). "CHF Mechanism in Flow Boiling from a Short Heated Wall – I. Examination of Near-Wall Conditions with the Aid of Photomicrography and High-Speed Video Imaging," *International Journal of Heat and Mass Transfer*, **36**, pp. 2511-2526.

Gersey, C. O. and Mudawar, I. (1995). "Effects of Heater Length and Orientation on the Trigger Mechanism for Near–Saturated Flow Boiling Critical Heat Flux – I. Photographic Study and Statistical Characterization of the Near–Wall Interfacial Features," *International Journal of Heat and Mass Transfer*, **38**, pp. 629-641.

Gersey, C. O. and Mudawar, I. (1995). "Effects of Heater Length and Orientation on the Trigger Mechanism for Near–Saturated Flow Boiling Critical Heat Flux – II. Critical Heat Flux Model," *International Journal of Heat and Mass Transfer*, **38**, pp. 643-654.

Howard, A. H. and Mudawar, I. (1999). "Orientation Effects on Pool Boiling Critical Heat Flux (CHF) and Modeling of CHF for Near-Vertical Surfaces," *International Journal of Heat and Mass Transfer*, **42**, pp. 1665-1688.

Katto, Y. (1978). "Generalized Correlation for Critical Heat Flux of Natural Convective Boiling in Confined Channels," *Transaction of JSME (in Japanese),* **44**, pp. 3908-3911.

Katto, Y. and Kosho, Y. (1979). "Critical Heat Flux of Saturated Natural Convection Boiling in a Space Bounded by Two Horizontal Co-Axial Disks and Heated from Below," *International Journal of Multiphase Flow*, **5**, pp. 219-224.

Kim, S. H., Baek, W. P. and Chang, S. H. (2000). "Measurements of Critical Heat Flux for Narrow Annuli Submerged in Saturated Water," *Nuclear Engineering and Design*, **199**, pp. 41-48.

Kim, Y. H. and Suh, K. Y. (2000). "Sensitivity Analyses for Maximum Heat Removal from Debris in the Lower Head," *Journal of the Korean Nuclear Society*, **32**(4), pp. 392-406.

Monde, M., Kusuda, H. and Uehara, H. (1982). "Critical Heat Flux During Natural Convective Boiling in Vertical Rectangular Channels Submerged in Saturated Liquid," *Transaction of ASME, Journal of Heat Transfer*, **104**, pp. 300-303.

Suh, K. Y. and Henry, R. E. (1996a). "Debris Interactions in Reactor Vessel Lower Plena during a Severe Accident - I. Predictive Model," *Nuclear Engineering and Design*, **166**, pp. 147-163.

Suh, K. Y. and Henry, R. E. (1996b). "Debris Interactions in Reactor Vessel Lower Plena During a Severe Accident - II. Integral Analysis," *Nuclear Engineering and Design*, **166**, pp. 165-178.

Xia, C., Hu, W. and Guo, Z. (1996). "Natural Convective Boiling in Vertical Rectangular Narrow Channels," *Experimental Thermal Fluid Science*, **12**, 313-324.

Yang, S. H., Baek, W. P. and Chang, S. H. (1997). "Pool Boiling Critical Heat Flux of Water on Small Plates: Effects of Surface Orientation and Size," *International Communications in Heat and Mass Transfer*, **24**, pp. 1093-1102.

Mudawar, I., Howard, A. H. and Gersey, C. O. (1997). "An Analytical Model for Near-Saturated Pool Boiling Critical Heat Flux on Vertical Surfaces,"*International Journal of Heat and Mass Transfer*, **40**, pp. 2327-2339.